# Oil Spill Candidate Detection from SAR Imagery Using a Thresholding-Guided Stochastic Fully-Connected Conditional Random Field Model

Anonymous EARTHVISION submission

Paper ID ****

## Abstract

*The detection of marine oil spill candidate from synthetic aperture radar (SAR) images is largely hampered by SAR speckle noise and the complex marine environment. In this paper, we develop a thresholding-guided stochastic fully-connected conditional random field (TGSFCRF) model for inferring the binary label from SAR imagery. First, an intensity thresholding approach is used to estimate the initial labels of oil spill candidates and the background. Second, a Gaussian mixture model (GMM) is trained using all the pixels based on the initial labels. Last, based on the GMM model, a graph-cut optimization approach is used for inferring the final labels. By using a threholding-guided approach, TGSFCRF can exploit the statistical characteristics of the two classes for better label inference. Moreover, by using a stochastic clique approach, TGSFCRF efficiently addresses the global-scale spatial correlation effect, and thereby can better resist the influence of SAR speckle noise and background heterogeneity. Experimental results on RADARSAT-1 ScanSAR imagery demonstrate that TGSFCRF can accurately delineate oil spill candidates without committing too much false alarms.*

## 1. Introduction

Spaceborne synthetic aperture radar (SAR), due to its ability to cover large areas irrespective of weather condition or sun-light illumination, provides a powerful tool for the detection of marine oil spill, which is usually caused by ships or drilling platforms, and greatly endanger the marine ecosystem. Efficient identification of potential oil spills from SAR imagery is crucial for supporting quick response to oil pollution and the cleanup efforts. The first use of SAR image for oil spill monitoring was by Elachi [1], who investigated the feasibility of Seasat imagery for oil spill detection. After the launch of the second generation of satellite SAR sensors in the 1990s, such as ENVISAT, ERS-2, and RADARSAT-1, SAR images became extensively used for oil spill detection [2–8]. The third generation of SAR sensors were launched in the past five years, such as Canadian RADARSAT-2, Italian Cosmo-Skymed, German TerraSAR-X and Japanese ALOS. These sensors are characterized by multi-polarization options, higher spatial resolution and shorter revisit time, therefore, provide better capability for oil spill detection [9, 10].

Today, almost all of the operational marine monitoring programs depend on trained human analysts to determine oil spill candidates, by visual interpretation, based on their experiences and prior knowledge [11]. However, dealing with a large amount of SAR images of vast marine regions is costly and time-consuming. As such, automatic methods for oil spill detection have been a very active research topic in remote sensing community. In the last two decades, efforts have been made by several organizations towards the development of semi-automated or fully automated systems for oil spill detection based on SAR imagery. Examples include the semi-automated systems such as Ocean Monitoring Workstation (OMW) at CIS [2], Alaska SAR Demonstration (AKDEMO) system [12], the European Commission Joint Research Centre (JRC) system [13], the Norwegian Defense Research Establishment (NDRE) system [14], and a fully-automated Kongsberg Satellite Services (KSAT)s oil spill detection system at Norway [15].

Oil spills appear as dark-spots on SAR imagery. However, other natural or man-made phenomena (e.g., organic film and low wind area), called look-alikes, also appear as dark-formations on SAR ocean images [16]. It is difficult to discriminate oil spills from look-alikes solely based on SAR intensity values. Ancillary features regarding dark-spots (e.g., texture, geometric shape, contrast with surrounding areas and contextual information) has to be extracted to further classify oil spills from look-alikes [17]. As a result, an oil spill identification system typically requires three stages: (i) oil spill candidate detection, (ii) feature extraction, and (iii) classification [18]. The first step aims to detect from SAR imagery all dark-spots that are potential oil spills. This step is very important for the system, because once oil spills are omitted in this step, they will never be detected in the following steps. Moreover, the false detections in the first step steps will increase the computational burden and classification difficulty of the subsequent steps.

This paper therefore focuses on developing effective oil spill candidate detection algorithm. Several approaches have been proposed for oil spill candidate detection. The commonly used approaches are based on intensity thresholding. Many global thresholds have been proposed: Nirchio et al. set the threshold as the normalized radar cross section (NRCS) minus standard deviation of the SAR image; Fiscella et al. used half of the averaged NRCS [7]. Although the global thresholding methods have high computational efficiency, they sometimes fail to detect weak oil spill candidate because the global thresholds do not always account for the local variation. By selecting the threshold locally, adaptive thresholding methods tend to be able to delineate oil spill candidates more accurately. Solberg et al. set the threshold to be $k$ dB below the mean value estimated in a moving window [4, 15, 19]. In order to resist the influence of speckle noise, Shu et al. proposed a thresholding method that takes advantage of spatial density information [20]. Another approach exploits the edge information on SAR image for oil spill detection. Chen et al. proposed the use of both Difference of Gaussian (DoG) and Laplace of Gaussian (LoG) to detect the boundary of oil spills [21]. As a band pass filter, the wavelet method was used for the delineation of oil spill areas [22–24]. Other more sophisticated oil spill candidate detection methods have been proposed, such as the neural network based approach [25] and the marked point process based approach [26].

The effectiveness of an oil spill candidate detection system depends highly on its capability to deal with the difficulties caused by the complex marine environment and the SAR speckle noise. The separability between the oil spill candidate class and the background class is usually very low, due to the variation caused by SAR speckle noise and the low intensity contrast between oil spill candidate and the background. Given the low class separability, the thresholding approaches tend to produce intense false detection and omissions, and the edge detection approaches could not accurately delineate the target boundaries. Moreover, because of the heterogeneity of the background, a unsupervised segmentation approach tend to split the big class of background into two small classes, leading to failure in oil spill candidate detection. In order to increase the class separability, the spatial contextual information in SAR image has to be exploit to resist the influence of speckle noise and to highlight the difference between the target and the background. Although oil spill candidates are weak signals, they tend to present significant patterns when being examined on large spatial scale. Consequently, the model accounting for large-scale spatial correlation effect is more suitable for oil spill candidate detection.

The paper presents thresholding-guided stochastic fully-connected conditional random field (TGSFCRF) algorithm for oil spill candidate detection. Comparing with ordinary conditional random field (CRF) that only consider the correlation effect in a small neighborhood, the fully-connected CRF (FCRF) can address correlation effect in the global image scale. However, FCRF usually requires huge computational cost. The TGSFCRF model can maintain the advantage of FCRF, but reduce its computational cost by using a stochastic clique approach, where the connectivity of a node with all the other nodes in the graph is determined in a stochastic manner [27]. Since oil spill candidates are usually weak signals and can be easily misclassified under a totally unsupervised circumstance. We therefore adopt a thresholding-guided approach to regulate the learning process. The experiments on RADARSAT-1 SAR imagery indicate that the proposed algorithm can accurately delineate oil spill candidate comparing with other methods.

The rest of the paper is organized as below. Section II describes the TGSFCRF model and its implementation. Section III presents the experiments results on RADARSAT-1 SAR images. Section IV concludes the study.

## 2. Methodology

In this section, we start with a introduction to TGSFCRF framework in the context of SAR oil spill candidate detection, followed by the detailed illustration of key components in TGSFCRF.

### 2.1. TGSFCRF Framework

TGSFCRF is a fully-connected random field model, where threholding approach is used as a guide to learn model parameters, and the stochastic clique is used to determine the connectivity among nodes in a fully-connected graph.

Let $x_i$ and $y_i$ denote respectively the intensity observation and the class label of a site in the SAR image lattice $I$ contains $|I| = N$ sites. The SAR image is expressed as $X = \{x_i | i \in I\}$ and the labels corresponding to this observation as $Y = \{y_i | i \in I\}$. Oil spill candidate detection aims to infer $Y$ given $X$ by maximizing the following conditional probability distribution:

$$P(Y|X) = \frac{1}{Z(X)} \exp\Big( -\sum_i \psi_u(y_i, X) - \sum_{(i,j)\in C} \psi_p(y_i, y_j, X)\Big) \tag{1}$$

where $Z(X)$ is the partition function, $\psi_u$ and $\psi_p$ are the unary potential and the pairwise potential respectively and $C$ encodes the set of clique structure in the random field. The clique structure $C$ in (1) determines the connectivity among nodes in the neighborhood. Since the the underlying graph is assumed to be fully-connected, the neighborhood of node $i$ denoted by $\mathcal{N}_i$, has the following expression:

$$\mathcal{N}_i = \{j | j = 1 : N, j \neq i\} \tag{2}$$

Based on the above model definition, the following two problems need to be addressed for effective oil spill candidate detection. First, performing oil spill detection is a totally unsupervised manner is not appropriate, because oil spill candidate are weak signals that usually constitute limited number of pixels comparing with the background. Considering the heterogeneity of the background, a unsupervised segmentation approach tend to split the big class of background into two small classes, leading to failure in oil spill candidate detection. Due to this reason, we adopt a threholding-guided approach to learn Gaussian statistics that can describe what the two classes look like. Based on this information, better oil spill candidate description can be achieved. Second, the heterogeneity of the background in SAR image and the variation in the spatial structure of oil spill candidates call for spatial models that are capable of modeling long-range spatial correlation effect. Nevertheless, modeling long-range correlation effect usually cause very high computational cost. Due to this reason, we use a stochastic clique approach which selects the most relevant pixels for building connectivity from the global image space.

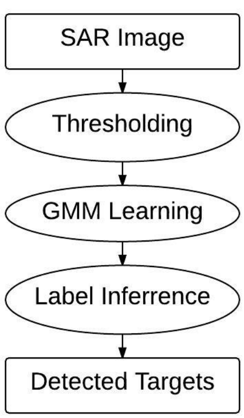


Figure 1. The flowchart of TGSFCRF.

As shown by Fig. 1, in TGSFCRF, an intensity thresholding approach is first conducted to estimate the initial estimation of binary labels, based on which, a Gaussian mixture model (GMM) involving the oil spill candidate class and the background class are learned. Based on GMM and a stochastic clique structure, a graph-cut approach is used to optimize the objective function of TGSFCRF, leading to the final estimation of the class labels.

In the following sections, we illustrate some key components in TGSFCRF algorithm, as well as the optimization scheme.

### 2.2. Intensity Thresholding

The initial class label of the pixel at the $i$th site is achieved by performing an intensity thresholding approach, according to the following rule:

$$y_i^0 = \begin{cases} 1 & \text{if } x_i \geqslant thrd \\ 0 & \text{otherwise.} \end{cases} \tag{3}$$

where $thrd = mean(X) - \omega \cdot std(X)$ with $\omega$ usually being 1. Since different images tend to have different mean and standard deviation values, using $thrd$ can adapt to the individual histogram characteristics.

### 2.3. GMM Learning

The initial class labels $Y^0$ will be used to estimate the unknown parameters in the unary potential, which is formulated as below:

$$\psi_u(y_i, X) = -log\Big(p(y_i|x_i)\Big) \tag{4}$$

where $p(y_i|i_i)$ is the posterior probability of $y_i$ given $x_i$ based on a GMM. The parameters in GMM are estimated by the maximum likelihood (ML) approach.

### 2.4. Stochastic Clique

To take the advantage of large-range spatial information with feasible computational complexity, we adapt the stochastic clique approach in [27] for modeling the spatial correlation effect in SAR image.

Fig. 2 displays some examples of SAR oil spill candidate images. As demonstrated in Fig. 2(a), the oil spill candidate can have elongated structures, which implies long range spatial correlation effect. Fig. 2(b) and Fig. 2(c), however, indicate that oil spill candidate sometimes has a big dense structure. Therefore, modeling oil spill candidates by fixed clique structure is challenging due to the variation in the direction and scale of spatial correlation effect. However, determining the clique structure in a data-driven manner might be more appropriate. Consequently, TGSFCRF, where stochastic clique approach is used to sample the relevant clique connectivities from a fully-connected random field, can capture the useful spatial contextual information for enhancing the detectability of oil spill candidate.

The widely used pairwise clique structure is adopted here. The clique structure $C$ is a combination of individual stochastic clique structures $\{C(i)\}$ associated with different nodes in the random field:

$$C = \{C(i)\} \tag{5}$$

$$C(i) = \{(i,j) | j \in \mathcal{N}_i, \mathbb{1}_{\{i,j\}} = 1\} \tag{6}$$

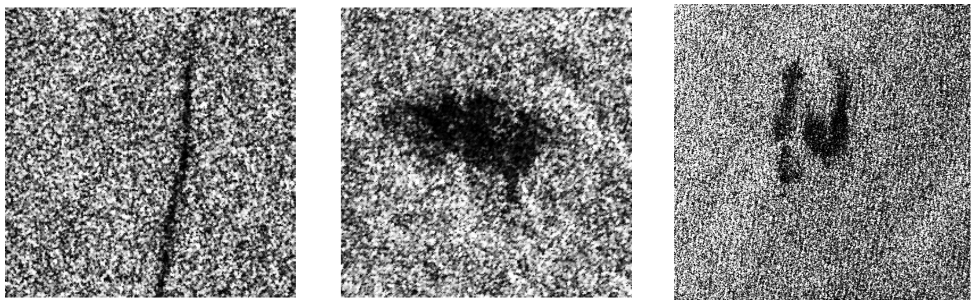

(a) (b) (c)

Figure 2. Examples of various image structures of oil spill candidates in SAR images. Oil spill candidates can have different shape structures, such as thin and elongated shape in (a) or dense and small shapes in (b), or a combination of some small spots that are near to each others in (c).

where $\mathbb{1}_{\{i,j\}} = 1$ is a clique indicator function determining whether two nodes $i$ and $j$ can construct a clique or not, according to a stochastic measure:

$$\mathbb{1}_{\{i,j\}} = \begin{cases} 1 & \text{if } \gamma \cdot P_{ij} Q_{ij} \geqslant \varphi \\ 0 & \text{otherwise.} \end{cases} \tag{7}$$

where $P_{ij}$ is the data similarity likelihood between pixel $x_i$ and $x_j$, $Q_{ij}$ is the probabilistic spatial closeness measurement from $x_i$ to $x_j$ in image space, $\gamma$ determines the sparsity of the graph, and $\varphi$ is a random value in the range of $[0, 1]$ generated from a uniform distribution.

Considering the noise distribution, the data similarity likelihood $P_{ij}$ between two amplitude values $a_i = \sqrt{x_i}$ and $a_j = \sqrt{x_j}$ is expressed as [28]:

$$P_{ij} = 4L \frac{\Gamma(2L-1)}{\Gamma(L)} \left( \frac{a_i a_j}{a_i^2 + a_j^2} \right)^{2L-1} \tag{8}$$

The probabilistic spatial closeness measurement $Q_{ij}$ between pixel $x_i$ and $x_j$ is defined as below:

$$Q_{ij} = exp \left( - \frac{(L_{ir} - L_{jr})^2 + (L_{ic} - L_{jc})^2}{2\sigma^2} \right) \tag{9}$$

where $L_{ir}$ and $L_{ic}$ are respectively the row and column locations of site $i$ in image space, and $\sigma$ determines the spatial scale.

Fig. 3 displays the graphical model of TGSFCRF, where the edge $e_{ik}$ between $y_i$ and $y_k$ is determined in a stochastic manner. Nodes that are closer in both feature space and image space have higher possibility to be connected, whereas nodes far away from each other have lower chance of being connected. As a result of implementing the criterion defined in (7), in TGSFCRF, only a subset of nodes in the neighborhood that are the most relevant with the referenced node will be adopted for building connectivity with the referenced node. TGSFCRF therefore can efficiently and effectively model large-scale spatial correlation effect.

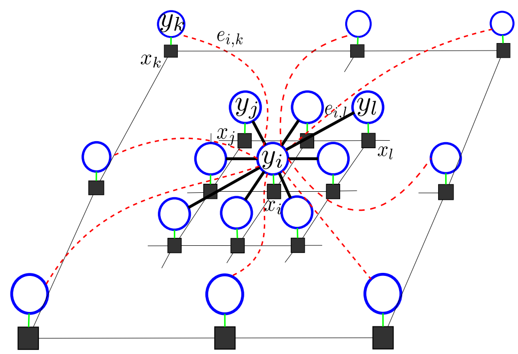


Figure 3. The graphical model of TGSFCRF. The probability of connectivity between the referenced node $y_i$ and an arbitrary node $y_k$ is denoted by edge $e_{ik}$. Closer nodes have black solid edges, indicating higher possibility to be connected, whereas nodes with far distance red dashed edges, implying a smaller chance for building connectivity.

## 2.5. MAP Inference

Since the unary potential can be achieved by GMM, to incorporate the spatial information, the pairwise potential is expressed as:

$$\psi_p(y_i, y_j, X) = -\lambda \cdot \mu(y_i, y_j) \cdot P_{ij} \tag{10}$$

where $\mu(y_i, y_j)$ is implemented according to the Potts model:

$$\mu(y_i, y_j) = \begin{cases} 1 & y_i \neq y_j \\ 0 & \text{otherwise.} \end{cases} \tag{11}$$

Using the above-described unary and pairwise potentials, the binary classification of SAR image into the oil spill candidate class and background class is achieved according to the maximum a posterior (MAP), such that

$$Y^* = \underset{\hat{Y}}{argmax} P(Y|X) \tag{12}$$

where $Y^*$ is the best label configuration in the set $\hat{Y}$ that maximizes $P(Y|X)$. To find $Y^*$, the energy function $\sum_i \psi_u(y_i, X) + \sum_{(i,j)\in C} \psi_p(y_i, y_j, X)$ of (1) is minimized by graph-cut approach. The stochastic clique scheme, as implemented in TGSFCRF, is seamlessly integrated into the conventional graph-cut based random field optimization framework by replacing the conventional clique with the stochastic clique.

The graph-cut [29, 30] algorithm divides the nodes in graph into two disjoint sets $Y_1$ and $Y_t$, with each set being connected to either the source terminal node $s$ or the sink terminal node $t$. The best partitioning of the nodes is the one that minimizes the cost of the cut, which is defined as the sum of weights on the edges being cut. Graph-cut can ideally fit in the problem here, because it can achieve global optimal solution for binary classification.

## 3. Results and Discussion

### 3.1. Dataset

Some RADARSAT-1 SAR images containing oil spill candidates provided by Canadian ice service (CIS) of Environment Canada are used for testing the proposed algorithm. In order to monitor the illegal release of oily wastes from ships traveling in Canadian waters, CIS has been designing a program called Integrated Satellite Tracking of Pollution (ISTOP) as part of its ice surveillance operational program towards effective use of RADARSAT images to aid oil spill detection. In ISTOP, human analysts at CIS manually interpret SAR images to detect oil spill candidates. The images provided by CIS are RADARSAT-1 ScanSAR intensity data, with HH polarization and a spatial resolution of 50×50 m. Sub-images containing both oil spill candidate and the surrounding sea area were clipped to test the proposed approach. The test dataset contains 21 images with various image size. This dataset covers major types of oil spill candidates detected under a variety of sea conditions.

### 3.2. Experimental Methods

The proposed TGSFCRF algorithm is tested on the RADARSAT-1 images to detect oil spill candidates. To examine the advantage of using the stochastic clique approach in TGSFCRF, we compare TGSFCRF with other two CRF approaches that use the same implementation with TGSFCRF but conventional pairwise clique structure defined in a neighborhood, i.e., TGCRF3 with 3×3 neighborhood and TGCRF11 with 11×11 neighborhood. Moreover, the threholding-guided GMM (TGGMM) model is also used to show the performance difference with CRF-based approaches when spatial contextual information is not addressed. For each method, the model parameter values are optimized by tuning the parameters using a random subset of 5 images before the experiments until the best visual detection results were achieved.

To quantitatively assess the accuracy of the detection results, a reference dataset was produced by manual image-interpretation to be used as ground-truth. To quantify the inconsistency between the detected target and the ground-truth target, we use three statistics, i.e., omission error (CE), commission error (OE), and averaged error (AE) [31]. First, CE measures the ratio of falsely-detected target relative to all detections:

$$CE = \frac{A_E - A_{EinR}}{A_E} \tag{13}$$

where $A_E$ and $A_R$ denote respectively the size of detected target and the size of ground-truth target, and $A_{EinR}$ is the size of detected target within a certain distance of the ground-truth target. Second, the OE measures the ratio of the omission in detections relative to the ground-truth target.

$$OE = \frac{A_R - A_{RinE}}{A_R} \tag{14}$$

where $A_{RinE}$ is the size of ground-truth target within a certain distance of the detected target. Last, AE is expressed as below:

$$AE = \frac{CE + OE}{2} \tag{15}$$

AE therefore measures the balanced detection capability of different methods by averaging CE and OE.

### 3.3. Results Analysis

Fig. 4 shows the oil spill candidate detection results achieved by different methods on several RADARSAT-1 Images. Due to the existence of speckle noise and the low contrast between oil spill candidates and the background, the TGGMM approach tends to produce many false detections. Comparing with TGGMM, TGCRF3 is less affected by the speckle noise and greatly reduces false alarms, indicating the benefits of considering spatial contextual information for label inference. Nevertheless, TGCRF3 tends to be easily disturbed by the background heterogeneity, and wrongly classified some dark areas in the background as oil spill candidates. This demonstrate the limitation and weakness of modeling local-scale spatial correlation effect when dealing with the complexity and unstationaries of SAR oil spill candidate images. This conclusion is reinforced by the fact that TGCRF11, which address larger-range correlation effect, is able to effectively resists the influence of background heterogeneity and produce relatively clean background. However, since TGCRF11 uses all the pixels in the neighborhood to connect with the center pixel, it faces the risk of accepting many pixels that are irrelevant to the center pixel for building connectivity, considering the disturbance of noise effect on the similarity measures. This may explain that fact that TGCRF11 undesirably keeps many dark pixels in the background and tends to blur the boundaries. Comparing with TGCRF3 and TGCRF11, TGSFCRF can better delineate the target without being significantly affected by the background heterogeneity and speckle noise, demonstrating the benefits and importance of modeling large-scale spatial correlation effect by determining the clique structure in a stochastic data-driven manner.

Table 1 shows the statistics of the numerical measures achieved by different methods on the 21 RADARSAT-1 SAR images. The statistics are basically consistent with the visual detection results. Overall, TGSFCRF achieves lower mean OE values, and much lower mean CE and AE values than TGCRF3 and TGCRF11, indicating a good balance between the ability to detect the target and the ability to resist the influence of the disturbance caused background heterogeneity. According to mean AE value, the second best method is TGCRF11, which achieves lower mean CE value, but slightly higher OE than TGCRF3. All CRF-based approach produce lower mean AE value than TGGMM approach, which stably achieve very high OE and CE values on the test images.

## 4. Conclusions

In this paper, we presented TGSFCRF algorithm for the purpose of oil spill candidate detection. First, the initial labels of oil spill candidate and the background are obtained by perofrming intensity threholding on SAR image. Second, the initial labels are used to train a GMM model. Third, using the GMM model, TGSFCRF is performed on SAR image again to infer the binary labels to achieve the task of oil spill candidate detection. Comparing the CRF and FCRF, TGSFCRF is more capable effectively modeling large-scale spatial correlation effect by the use of stochastic clique approach, and thereby is more tailored to the characteristics of SAR oil spill candidates. The TGSFCRF is solved by a graph-cut approach to achieve global optimal for the binary label problem. The experiments conducted on many RADARSAT-1 ScanSAR images demonstrate that TGSFCRF better delineate oil spill candidate, without being significantly affected by background and foreground heterogeneities caused by SAR speckle noise and the complex marine environment.

## 5. Acknowledgements

This work is partly funded by the Natural Sciences and Engineering Research Council of Canada (NSERC) and the Canadian Space Agency (CSA). This research was undertaken, in part, thanks to funding from the Canada Research Chairs program.

## References

[1] C. Elachi, "Spaceborne imaging radar: geologic and oceanographic applications," *Science*, vol. 209, no. 4461, pp. 1073–1082, 1980. 1

[2] M. D. Henschel, R. Olsen, P. Hoyt, and P. W. Vachon, "The ocean monitoring workstation: experience gained with RADARSAT," *Geomatics in the ERA of RADARSAT (GER97)*, 1997. 1

[3] A. H. S. Solberg and E. Volden, "Incorporation of prior knowledge in automatic classification of oil spills in ERS SAR images," in *Geoscience and Remote Sensing, 1997. IGARSS'97. Remote Sensing-A Scientific Vision for Sustainable Development., 1997 IEEE International*, vol. 1. IEEE, 1997, pp. 157–159. 1

[4] A. S. Solberg, G. Storvik, R. Solberg, and E. Volden, "Automatic detection of oil spills in ERS SAR images," *Geoscience and Remote Sensing, IEEE Transactions on*, vol. 37, no. 4, pp. 1916–1924, 1999. 1, 2

[5] H. Espedal, "Satellite SAR oil spill detection using wind history information," *International Journal of Remote Sensing*, vol. 20, no. 1, pp. 49–65, 1999. 1

[6] H. Espedal and O. Johannessen, "Cover: Detection of oil spills near offshore installations using synthetic aperture radar (sar)," 2000. 1

[7] B. Fiscella, A. Giancaspro, F. Nirchio, P. Pavese, and P. Trivero, "Oil spill detection using marine SAR images," *International Journal of Remote Sensing*, vol. 21, no. 18, pp. 3561–3566, 2000. 1, 2

[8] F. Del Frate, A. Petrocchi, J. Lichtenegger, and G. Calabresi, "Neural networks for oil spill detection using ERS-SAR data," *Geoscience and Remote Sensing, IEEE Transactions on*, vol. 38, no. 5, pp. 2282–2287, 2000. 1

[9] A. Gambardella, M. Migliaccio, and G. De Grandi, "Wavelet polarimetric SAR signature analysis of sea oil spills and look-alike features," in *Geoscience and Remote Sensing Symposium, 2007. IGARSS 2007. IEEE International*. IEEE, 2007, pp. 983–986. 1

[10] V. V. Malinovsky, S. Sandven, A. S. Mironov, and A. E. Korinenko, "Identification of oil spills based on ratio of alternating polarization images from ENVISAT," in *Geoscience and Remote Sensing Symposium, 2007. IGARSS 2007. IEEE International*. IEEE, 2007, pp. 1326–1329. 1

[11] Z. Ou, D. Abreu *et al.*, "Integrated satellite tracking of pollution: a new operational program," in *2007 IEEE International Geoscience and Remote Sensing Symposium*, 2007, pp. 967–970. 1

[12] W. G. Pichel and P. Clemente-Colón, "NOAA CoastWatch SAR applications and demonstration," *Johns Hopkins APL technical digest*, vol. 21, no. 1, pp. 49–57, 2000. 1

[13] G. Ferraro, A. Bernardini, M. David, S. Meyer-Roux, O. Muellenhoff, M. Perkovic, D. Tarchi, and K. Topouzelis, "Towards an operational use of space imagery for oil pollution monitoring in the Mediterranean basin: A demonstration in the Adriatic sea," *Marine Pollution Bulletin*, vol. 54, no. 4, pp. 403–422, 2007. 1

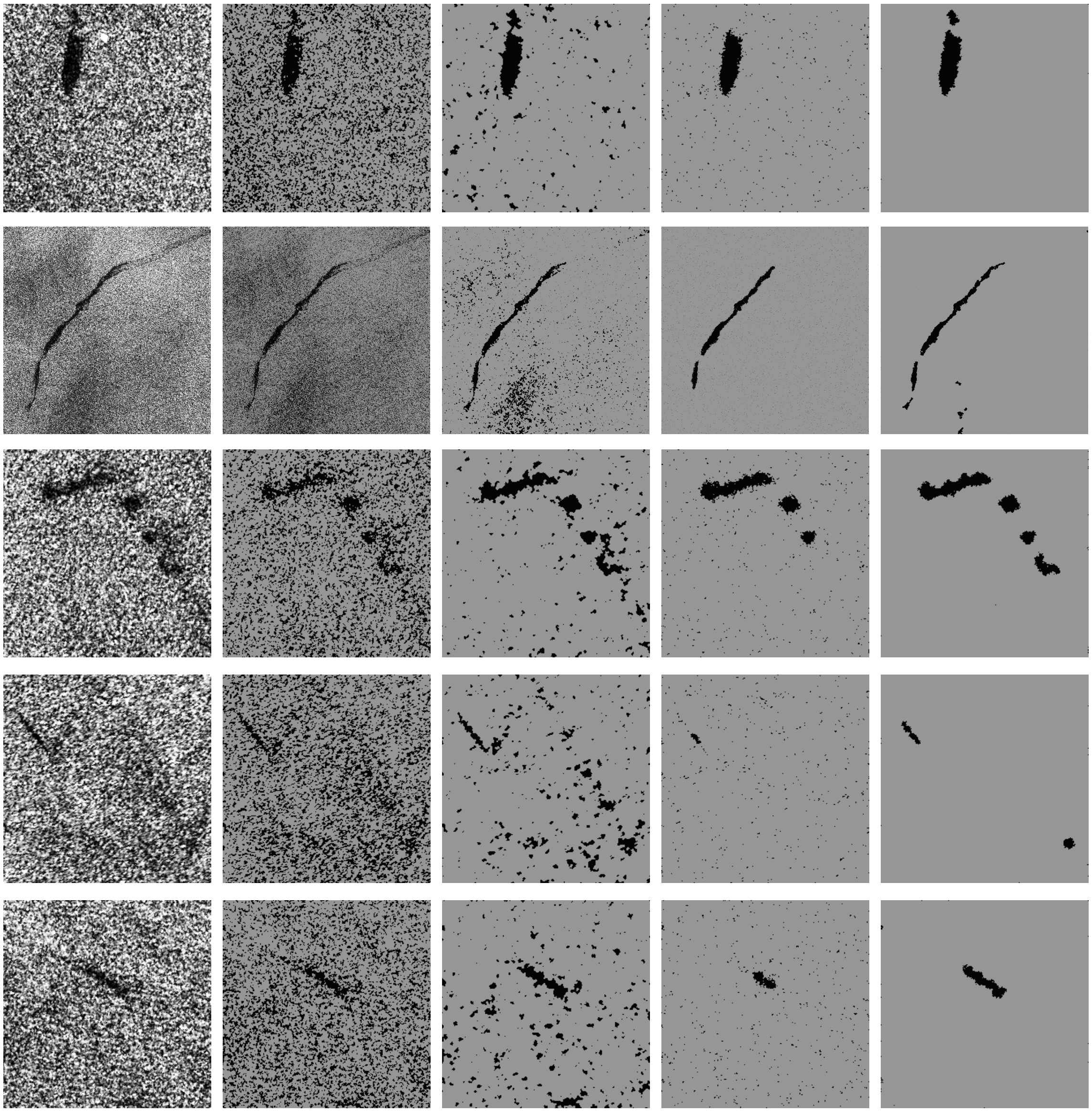


Figure 4. The detection results achieved by different methods on several RADARSAT-1 images. For display purpose, the SAR images in the first column have been enhanced by performing histogram equalization on the original SAR images. TGGMM method tends to produce intense false detection. TGCRF3 performs better than TGGMM, but is still affected by background heterogeneity and yields many false alarms. TGCRF11 tends to erase the boundaries and keep undesirable black dots in the background. TGSFCRF can accurately identify the targets and produce a clean background.

Table 1. Statistics (i.e., mean, median, standard deviation) of omission error (OE), commission error (CA) and averaged error (CA) achieved by different methods on 21 RADARSAT-1 SAR oil spill candidate images. For all statistics, lower values indicate better performance.

| | OE | | CE | | AE | |
|---|---|---|---|---|---|---|
| | Mean (%) | Std. (%) | Mean (%) | Std. (%) | Mean (%) | Std. (%) |
| TGSFCRF | 10.2 | 22.9 | **11.2** | 19.9 | **10.7** | 21.4 |
| TGGMM | 15.1 | **8.7** | 91.7 | **7.8** | 53.4 | **8.2** |
| TGCRF3 | **9.0** | 9.5 | 70.7 | 18.1 | 39.9 | 13.8 |
| TGCRF11 | 14.3 | 21.7 | 46.6 | 31.0 | 30.4 | 26.4 |

[14] K. Eldhuset, “An automatic ship and ship wake detection system for spaceborne SAR images in coastal regions,” *Geoscience and Remote Sensing, IEEE Transactions on*, vol. 34, no. 4, pp. 1010–1019, 1996. 1

[15] A. H. S. Solberg, C. Brekke, and P. Ove Husoy, “Oil spill detection in Radarsat and Envisat SAR images,” *Geoscience and Remote Sensing, IEEE Transactions on*, vol. 45, no. 3, pp. 746–755, 2007. 1, 2

[16] P. Clemente-Colón and X.-H. Yan, “Low-backscatter ocean features in synthetic aperture radar imagery,” *Johns Hopkins APL Technical Digest*, vol. 21, no. 1, pp. 116–121, 2000. 1

[17] K. N. Topouzelis, “Oil spill detection by sar images: dark formation detection, feature extraction and classification algorithms,” *Sensors*, vol. 8, no. 10, pp. 6642–6659, 2008. 1

[18] C. Brekke and A. H. Solberg, “Oil spill detection by satellite remote sensing,” *Remote sensing of environment*, vol. 95, no. 1, pp. 1–13, 2005. 1

[19] A. H. Solberg, S. T. Dokken, and R. Solberg, “Automatic detection of oil spills in Envisat, Radarsat and ERS SAR images,” in *Geoscience and Remote Sensing Symposium, 2003. IGARSS’03. Proceedings. 2003 IEEE International*, vol. 4. IEEE, 2003, pp. 2747–2749. 2

[20] Y. Shu, J. Li, H. Yousif, and G. Gomes, “Dark-spot detection from SAR intensity imagery with spatial density thresholding for oil-spill monitoring,” *Remote Sensing of Environment*, vol. 114, no. 9, pp. 2026–2035, 2010. 2

[21] C. Chen, K. Chen, L. Chang, and A. Chen, “The use of satellite imagery for monitoring coastal environment in taiwan,” in *Geoscience and Remote Sensing, 1997. IGARSS’97. Remote Sensing-A Scientific Vision for Sustainable Development., 1997 IEEE International*, vol. 3. IEEE, 1997, pp. 1424–1426. 2

[22] A. K. Liu, C. Y. Peng, and S.-S. Chang, “Wavelet analysis of satellite images for coastal watch,” *Oceanic Engineering, IEEE Journal of*, vol. 22, no. 1, pp. 9–17, 1997. 2

[23] S. Wu and A. Liu, “Towards an automated ocean feature detection, extraction and classification scheme for SAR imagery,” *International Journal of Remote Sensing*, vol. 24, no. 5, pp. 935–951, 2003. 2

[24] S. Derrode and G. Mercier, “Unsupervised multiscale oil slick segmentation from sar images using a vector HMC model,” *Pattern Recognition*, vol. 40, no. 3, pp. 1135–1147, 2007. 2

[25] K. Topouzelis, V. Karathanassi, P. Pavlakis, and D. Rokos, “Detection and discrimination between oil spills and look-alike phenomena through neural networks,” *ISPRS Journal of Photogrammetry and Remote Sensing*, vol. 62, no. 4, pp. 264–270, 2007. 2

[26] Y. Li and J. Li, “Oil spill detection from SAR intensity imagery using a marked point process,” *Remote Sensing of Environment*, vol. 114, no. 7, pp. 1590–1601, 2010. 2

[27] M. Shafiee, A. Wong, P. Siva, and P. Fieguth, “Efficient bayesian inference using fully connected conditional random fields with stochastic cliques,” in *International Conference on Image Processing (ICIP). IEEE*, 2014, pp. 1–5. 2, 3

[28] C.-A. Deledalle, L. Denis, and F. Tupin, “Iterative weighted maximum likelihood denoising with probabilistic patch-based weights,” *Image Processing, IEEE Transactions on*, vol. 18, no. 12, pp. 2661–2672, 2009. 4

[29] L. Ford and D. Fulkerson, *Flows in networks*. Princeton Princeton University Press, 1962, vol. 1962. 5

[30] P. Kohli and P. Torr, “Dynamic graph cuts for efficient inference in markov random fields,” *IEEE Transactions on Pattern Analysis and Machine Intelligence,*, vol. 29, no. 12, pp. 2079–2088, 2007. 5

[31] C. Wiedemann, C. Heipke, H. Mayer, and O. Jamet, “Empirical evaluation of automatically extracted road axes,” *Empirical Evaluation Techniques in Computer Vision*, pp. 172–187, 1998. 5